LETTER

Super–catastrophic disruption of asteroids at small perihelion distances

Mikael Granvik[1,2], Alessandro Morbidelli[3], Robert Jedicke[4], Bryce Bolin[3,4], William F. Bottke[5], Edward Beshore[6], David Vokrouhlický[7], Marco Delbò[3] & Patrick Michel[3]

Most near-Earth objects came from the asteroid belt and drifted via non-gravitational thermal forces into resonant escape routes that, in turn, pushed them onto planet-crossing orbits[1–3]. Models predict that numerous asteroids should be found on orbits that closely approach the Sun, but few have been seen. In addition, even though the near-Earth-object population in general is an even mix of low-albedo (less than ten per cent of incident radiation is reflected) and high-albedo (more than ten per cent of incident radiation is reflected) asteroids, the characterized asteroids near the Sun typically have high albedos[4]. Here we report a quantitative comparison of actual asteroid detections and a near-Earth-object model (which accounts for observational selection effects). We conclude that the deficit of low-albedo objects near the Sun arises from the super-catastrophic breakup (that is, almost complete disintegration) of a substantial fraction of asteroids when they achieve perihelion distances of a few tens of solar radii. The distance at which destruction occurs is greater for smaller asteroids, and their temperatures during perihelion passages are too low for evaporation to explain their disappearance. Although both bright and dark (high- and low-albedo) asteroids eventually break up, we find that low-albedo asteroids are more likely to be destroyed farther from the Sun, which explains the apparent excess of high-albedo near-Earth objects and suggests that low-albedo asteroids break up more easily as a result of thermal effects.

Most near-Earth-object (NEO) discoveries during the past decade have been made by the Catalina Sky Survey (CSS), a combination of two distinct observatories with complementary capabilities. The 1.5-m Mt Lemmon telescope (code G96) typically detects faint NEOs close to the ecliptic, whereas the 0.8-m Catalina telescope (code 703) covers a larger area of the sky but focuses on brighter targets. From 2005 to 2012, CSS made 7,952 serendipitous detections of 3,632 distinct NEOs with absolute magnitudes H ranging from 17 to 25 during nights that had well established estimates for the detection efficiency. The detections were roughly equally shared between the two telescopes and the detected NEOs provide an extensive coverage of the parameter space (Supplementary Fig. 1).

We use the CSS NEO detections to constrain a model describing the true number of NEOs, $N(a, e, i, H)$, as a function of orbital parameters (semimajor axis a, eccentricity e and inclination i) and absolute magnitude H, a proxy for the physical size. Our new model of the NEO population is based on the methodology of ref. 3. First, we tracked the dynamical evolution of test asteroids from seven source regions or escape routes, s, in the main asteroid belt and nearby small-body reservoirs all the way into the inner Solar System (Supplementary Figs 2 and 3). Next, the orbital pathways followed by the bodies were assembled into source-specific steady-state orbital distributions, $R_s(a, e, i)$ (Supplementary Fig. 4). These functions were then multiplied by source-specific

parametric absolute-magnitude distributions, $N_s(H)$, and added together to produce $N(a, e, i, H)$. The model was then multiplied by the computed[5] observational selection effects of CSS, $B(a, e, i, H)$ (Supplementary Fig. 5), thus obtaining a biased NEO model $N(a, e, i, H) \times B(a, e, i, H)$. The free parameters describing the $N_s(H)$ functions were determined by best-fitting the biased NEO model to the distribution of thousands of NEO detections from the CSS, $n(a, e, i, H)$, thus yielding a new and improved NEO population model. These computations are described in greater detail in Supplementary Information.

The observed a, e, i and H distributions generally agree with the biased NEO model (Supplementary Fig. 6). The $q = a(1 - e)$ distribution reveals a systematic offset in that the model predicts too many NEOs with small q and too few with large q (Fig. 1). If we assume that the overprediction at $q \leq 0.6$ astronomical units (AU) is the real source for the discrepancy, then the underprediction at large q is a feature resulting from how we fit the model to the data: the absolute number of NEO detections is one of the constraints and therefore the method compensates for an overprediction at small q with an underprediction at large q. The discrepancy in the q distribution has not been noticed in the past because previous models were calibrated with much smaller samples of NEOs and the discrepancy was not statistically significant[6].

A possible explanation for the discrepancy is that the combination of orbital steady-state distributions $R_s(a, e, i)$ is not flexible enough to allow for a good fit at small q. To test this explanation we divided the test asteroids into a larger number N_s of source regions and re-did the analysis. It turns out that even a model with $N_s = 24$ (Supplementary Fig. 7) is unable to match the observed q distribution (Supplementary Fig. 8). To rule out systematic problems with our orbital steady-state distributions we also tried orbital steady-state distributions computed by others using different starting conditions and integration parameters[7]. The alternative orbital distributions resulted in an even worse fit to the observed data, at least partly explained by the smaller number of source regions considered (Supplementary Fig. 9), and do not solve the discrepancy in q (Supplementary Fig. 8).

To validate the adopted methodology and, in particular, the bias correction, we carried out two tests which made use of the fact that CSS is composed of two surveys, G96 and 703, with partly complementary capabilities. The first test was to fit separately to G96 and to 703 to identify problems in either one of the surveys or their estimated selection effects. The discrepancy in q is present in both cases (Supplementary Fig. 8) and we conclude that the discrepancy in q is not specific to the chosen survey. The second test was a cross-check of the results: we estimated model parameters by fitting just the data from 703 (G96) in the limited range 0.7 AU $< q < 1.3$ AU, used the resulting model and estimates for selection effects to predict the absolute number of detections for G96 (703) in the same q range, and compared the prediction to the data. The results show that the adopted methodology and bias corrections are sound

[1]Department of Physics, PO Box 64, 00014 University of Helsinki, Finland. [2]Finnish Geospatial Research Institute, PO Box 15, 02430 Masala, Finland. [3]Observatoire de la Cote d'Azur, Boulevard de l'Observatoire, F 06304 Nice Cedex 4, France. [4]Institute for Astronomy, University of Hawaii, 2680 Woodlawn Drive, Honolulu, Hawaii 96822, USA. [5]Southwest Research Institute, 1050 Walnut Street, Suite 300, Boulder, Colorado 80302, USA. [6]University of Arizona, 933 North Cherry Avenue, Tucson, Arizona 85721-0065, USA. [7]Institute of Astronomy, Charles University, V Holešovičkách 2, CZ 18000 Prague 8, Czech Republic.
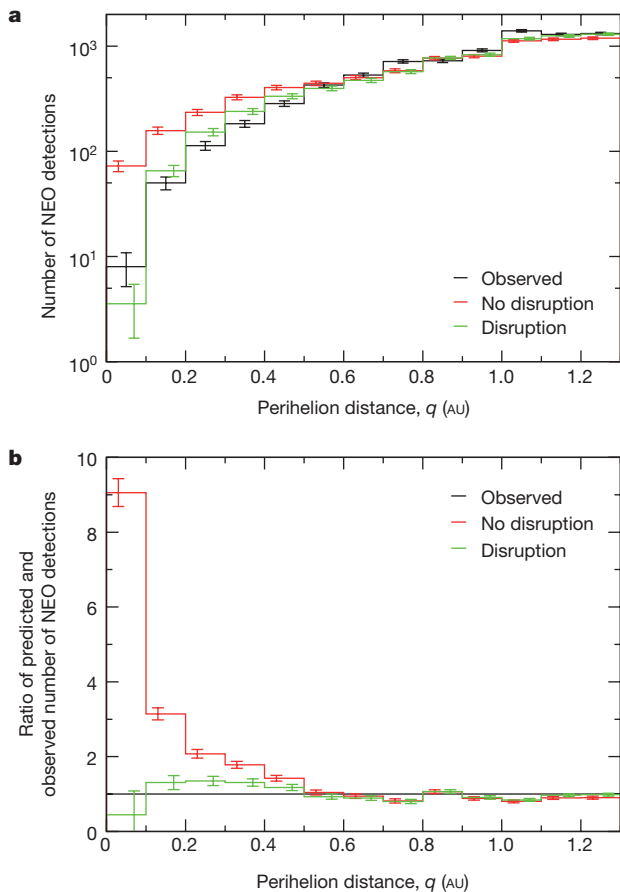
Figure 1 | Observed and predicted perihelion distances for NEOs detected by the CSS during 2005–2012. The observed perihelion distance distribution (black) compared with the biased model predictions with (green) and without (red), assuming a disruption at $\bar{q}_\star = 0.076$ AU. **a**, The observed and predicted number of NEO detections. **b**, The ratio between the observed and predicted number of NEO detections. The model without disruption shows a systematic overprediction at small q, whereas assuming a disruption breaks the trend and reproduces the observed q distribution. The s.e.m. error bars are computed assuming Poisson statistics.

and that the simultaneous use of complementary data sets leads to improved and more accurate models (Supplementary Fig. 10). Extrapolations to $q < 0.7$ AU systematically show that CSS should have discovered more NEOs on orbits with small q if such objects existed (Supplementary Fig. 8). We therefore conclude that some physical mechanism must be reducing the number of NEOs at small q.

We propose that when NEOs reach some critical perihelion distance, $q_\star$, they catastrophically disrupt. To test the proposed mechanism we constructed alternative orbital steady-state distributions by considering the dynamical evolution of test asteroids only until their q becomes smaller than a pre-defined value $q_\star$. The observed q distribution is best reproduced with $\bar{q}_\star = (0.0760 \pm 0.0025)$ AU $\approx (16 \pm 0.5)R_\odot$ (Fig. 1). Also the observed (a, e, i, H) distributions are accurately reproduced (Supplementary Fig. 11). The best-fit model predicts that there are $(7.32 \pm 1.33) \times 10^5$ NEOs with $17 < H < 25$ and $1{,}008 \pm 45$ NEOs with $H < 17.75$. Both numbers agree with the most recent estimates[8] (Supplementary Fig. 12). The best-fit model also reproduces the observed relative fractions of Amor (1.017 AU $< q \leq 1.3$ AU), Apollo ($a \geq 1$ AU and $q \leq 1.017$ AU) and Aten ($a < 1$ AU and aphelion distance $Q > 0.983$ AU) asteroids with $17 \leq H < 17.5$—the observed fractions are 47%, 50% and 3%, whereas the model predicts $43 \pm 5\%$, $53 \pm 5\%$ and $3.5 \pm 0.6\%$, respectively. See the Supplementary Video for an animation of how the orbit distribution changes with H.

To assess the effect of size on $\bar{q}_\star$, we divided the NEOs detected by CSS into three different groups as a function of H, and fitted $\bar{q}_\star$ separately to each of these groups. The result shows a clear trend of increasing $\bar{q}_\star$ with increasing H (Fig. 2), that is, an inverse correlation between $\bar{q}_\star$ and physical size. A direct consequence of the inverse correlation is that a kilometre-scale asteroid has to disrupt into fragments smaller than a few tens of metres in a single event or through a disruption cascade, depending on the disruption mechanism. The disruption distances are too large to be explained by tidal effects and evaporation[9]. While the average surface temperature of the sunlit hemisphere on mid-sized NEOs may surpass 900 K, the resulting diurnal heat waves will penetrate[10] only to depths of some tens of centimetres. Silicates immediately below the surface layer will therefore remain solid. This reveals that the actual disruption mechanism, although clearly related to temperature, is not trivial. A possibility is that rocks break into small grains by thermal cracking[11] and the grains are then blown away from the asteroid by radiation pressure[12]. Another possibility is that the
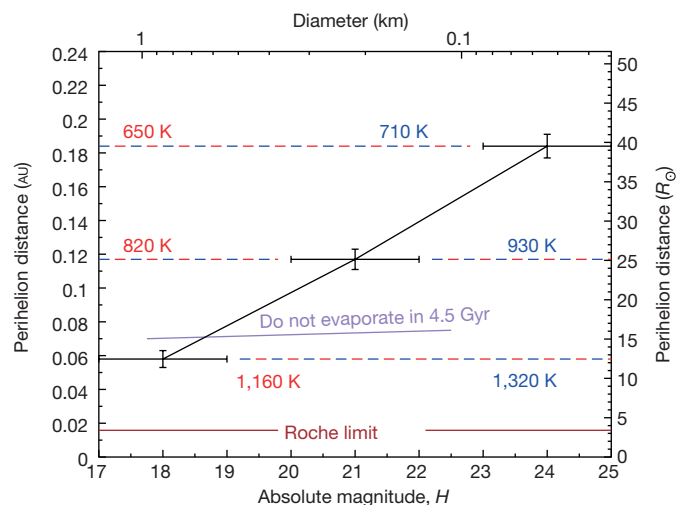

Figure 2 | Average disruption distance as a function of absolute magnitude and an asteroid's physical size. We split the NEO detections by CSS into three different H groups, with the H range shown by the horizontal error bars ($17 < H < 19$ contains 3,326 detections, $20 < H < 22$ contains 1,669 detections, and $23 < H < 25$ contains 913 detections). The average dynamical lifetime of NEOs is a few million years and asteroids on circular orbits with $r = \bar{q}_\star$ above the purple line will not have evaporated[9] after 4.5 billion years, the age of the Solar System. Evaporation can thus not explain the disappearance of small and mid-sized NEOs and, given the timescales, it is also an unlikely disruption mechanism for large NEOs. The brown horizontal line marks the Sun's Roche limit for a hypothetical fluid comet with a density of 0.5 g cm^{-3}, and serves as an approximate upper limit for tidal disruption of asteroids and comets. The red dashed lines correspond to the equilibrium temperature, $T_{eq} = [(1 - A)L_0/(16\pi\varepsilon\sigma r^2)]^{0.25}$, at perihelion, $r = q$, when assuming a Bond albedo of $A = 0.07$ and an infrared emissivity of $\varepsilon = 0.9$. $L_0 = 3.827 \times 10^{26}$ W is the solar luminosity and $\sigma = 5.6704 \times 10^8$ W m^{-2} K^{-4} is the Stefan–Boltzmann constant. The blue dashed lines correspond to the simple estimate of the temperature average over a sunlit hemisphere $T_{av} = 4T_{ss}/5$ with the subsolar temperature $T_{ss} = \sqrt{2}T_{eq}$. The true average surface temperature will lie somewhere between T_{eq} and T_{av}, because T_{eq} does not allow for local temperature variations and T_{av} does not account for conduction and sublimation. The conversion between H and diameter assumes a geometric albedo of 0.15. The detection-weighted average $\bar{q}_\star$ of the three groups is 0.094 ± 0.010 AU, which is about $24 \pm 17\%$ larger than the value obtained by fitting all groups simultaneously. The difference is a systematic error resulting from averaging over H. The line connecting the three groups emphasizes the linear (nonlinear) relation between the $\bar{q}_\star$ and H (diameter). The s.d. error bars on $\bar{q}_\star$ were estimated by generating 50 random representations of the best-fit model and re-fitting for $\bar{q}_\star$. We required that the solutions for $\bar{q}_\star$ must reproduce the observed q distribution: that is, all $\bar{q}_\star$ that were substantially larger than the smallest observed q were discarded.
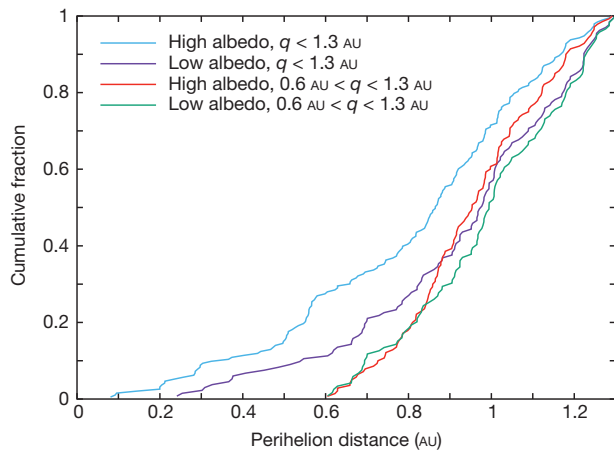
Figure 3 | Empirical distribution functions in perihelion distance for low-albedo and high-albedo NEOs detected by WISE. The WISE data set is biased against high-albedo NEOs: for a given absolute magnitude H, the higher the geometric albedo, the fainter the infrared apparent magnitude $W3$. The WISE detection efficiency is close to 100% up to $W3 = 9.5$, drops to 50% at $W3 = 10$ and is close to zero beyond[22] $W3 = 10.5$. This means that asteroids with large enough albedos would not have been observed by WISE. To correct for the WISE albedo bias we assume that its limiting magnitude is $W3_{lim} = 10$. Then, for each NEO with a WISE-determined albedo we identify all its WISE-reported observations at different epochs, select the smallest apparent magnitude $W3_{min}$ of all reported values, and reject that NEO from consideration if $W3_{min} > W3_{lim}$. This reduces the initial number of 394 NEOs to 326 with $W3_{lim} = 10$ and $H > 15$, the latter requirement ensuring that the albedos correspond to relatively small NEOs. The Anderson–Darling test applied to empirical distribution functions in q shows that it is extremely unlikely that the 133 low-albedo and 193 high-albedo NEOs have a common parent distribution ($p \approx 0.0003$) when accounting for $q < 1.3$ AU. A common origin for the q distributions becomes reasonable when limiting the analysis to NEOs with 0.6 AU $< q < 1.3$ AU only, that is, 119 low-albedo and 140 high-albedo NEOs ($p \approx 0.12$).

anisotropic emission of thermal photons[13] or the scattering of sublimating gas molecules[14] cause the asteroids to spin faster, to the point when gravity and cohesive forces can no longer keep them intact. A third possibility is that all asteroids contain volatile elements that, when sublimating at a moderate temperature, exert enough pressure on the body to blow it up.

To gain insight into the process leading to asteroid disruption, we investigated whether asteroids with different surface properties behave differently. For this purpose, we compared the q distributions of low-albedo and high-albedo NEOs detected by the Wide-field Infrared Survey Explorer (WISE) mission. The Anderson–Darling test[15] shows that the probability that these two samples come from a common parent distribution is only 0.03%, whereas a reasonable agreement is found when limiting the analysis to NEOs with $q > 0.6$ AU (Fig. 3). This result agrees with the results of an independent analysis[4] of WISE data, which showed that the observed Aten asteroids have, on average, higher albedos than Apollo and Amor asteroids. This can be explained if low-albedo NEOs disrupt, on average, farther from the Sun than high-albedo asteroids of comparable size, implying that they have different physical properties that make them more vulnerable to strong solar irradiation. The fact that the q distribution of low-albedo NEOs appears to be steeper than that of high-albedo NEOs at $q < 0.6$ AU supports this conclusion: the larger q_* is, the steeper is the resulting q distribution (Supplementary Fig. 13). A larger average disruption distance may be due to a higher volatile budget in low-albedo asteroids, as suggested by the composition of the most primitive carbonaceous meteorites (usually expected to be related to these bodies) and by the quite common presence of hydration bands in their spectra. Thermal cracking is also more efficient for carbonaceous meteorites than for ordinary chondrites (the meteorites associated with high-albedo asteroids). We also

note that darker NEOs experience somewhat greater heating and may therefore be more prone to thermally driven disruption.

In our model we assume that an instantaneous disruption takes place when $q \leq \bar{q}_*$ for an NEO. We predict that NEO disruptions must take place in less than 250 years, the timescale used to record our model data. Our results are consistent with the (q, H) distribution of known asteroids. Asteroid (394130) 2006 HY_{51} has the smallest perihelion distance, $q \approx 0.081$ AU $\approx 17.4 R_\odot$, among known NEOs with reliable estimates for the absolute magnitude. Its absolute magnitude, $H = 17.2$, is in agreement with our assessment of the average disruption distance (Fig. 2). Our results are also in agreement with observations of a slow erosion of the asteroid (3200) Phaethon[16], which is too large to disrupt catastrophically on its current orbit.

The recorded inclination distribution of test asteroids at the disruption epoch overlaps with the observed inclination distribution of $q < 0.184$ AU meteor showers identified in data obtained by the Canadian Meteor Orbit Radar[17,18] (CMOR; Supplementary Fig. 14). While covering the same range, the latter distribution is skewed towards larger values, which can be understood considering that radar is more sensitive to high-speed meteors and hence the orbital distribution is biased against low-inclination orbits. Super-catastrophic disruptions are consistent with the fact that parent bodies have yet to be detected for most meteor streams with small q and small i identified in CMOR data. Given the inverse correlation between $\bar{q}_*$ and asteroid diameter we predict that the average total mass of meteor streams lacking obvious parent bodies should diminish as a function of q as long as $q \leq 0.2$ AU and $i \leq 40°$.

In the future, a detailed understanding of the circumstances leading to disruption of asteroids at different q values may offer insight into their bulk composition as well as internal structure. In particular, a quantitative assessment of the volatile content for NEOs, and hence of their siblings in the main asteroid belt, by mapping out the disruption probability as a function of q and source region, would complement current approaches, which usually rely on extrapolation from surface properties[19] and the detection of comet-like activity[20,21].

1. Morbidelli, A. & Vokrouhlický, D. The Yarkovsky-driven origin of near Earth asteroids. *Icarus* **163,** 120–134 (2003).
2. Morbidelli, A., Bottke, W. F. Jr, Froeschlé, C. & Michel, P. Origin and evolution of near-Earth objects. *Asteroids* **III,** 409–422 (2002).
3. Bottke, W. F., Jedicke, R., Morbidelli, A., Petit, J.-M. & Gladman, B. Understanding the distribution of near-Earth asteroids. *Science* **288,** 2190–2194 (2000).
4. Mainzer, A. *et al.* Characterizing subpopulations within the near-Earth objects with NEOWISE: preliminary results. *Astrophys. J.* **752,** 110 (2012).
5. Jedicke, R., Bolin, B., Granvik, M. & Beshore, E. A fast method for quantifying observational selection effects in asteroid surveys. *Icarus* **266,** 173–188 (2016).
6. Bottke, W. F. *et al.* Debiased orbital and absolute magnitude distribution of the near-Earth objects. *Icarus* **156,** 399–433 (2002).
7. Greenstreet, S., Ngo, H. & Gladman, B. The orbital distribution of near-Earth objects inside Earth's orbit. *Icarus* **217,** 355–366 (2012).
8. Harris, A. W. & D'Abramo, G. The population of near-Earth asteroids. *Icarus* **257,** 302–312 (2015).
9. Campins, H., Davis, D. R., Weidenschilling, S. J. & Magee, M. in *Completing the Inventory of the Solar System* (eds Rettig, T. & Hahn, J. M.) *Astron. Soc. Pacif. Conf. Ser.* **107,** 85–96 (1996).
10. Lewis, J. S. *Physics and Chemistry of the Solar System* 257–259 (Elsevier Academic Press, 2004).
11. Delbo, M. *et al.* Thermal fatigue as the origin of regolith on small asteroids. *Nature* **508,** 233–236 (2014).
12. Jewitt, D. The active asteroids. *Astron. J.* **143,** 66 (2012).
13. Vokrouhlický, D., Bottke, W. F., Chesley, S. R., Scheeres, D. J. & Statler, T. S. The Yarkovsky and YORP effects. *Asteroids* **IV,** 509–531 (2015).
14. Steckloff, J. K. & Jacobson, S. A. The formation of striae within cometary dust tails by a sublimation-driven YORP-like effect. *Icarus* **264,** 160–171 (2016).
15. Feigelson, E. D. & Jogesh Babu, G. *Modern Statistical Methods for Astronomy* 105–117 (Cambridge Univ. Press, 2012).
16. Jewitt, D., Li, J. & Agarwal, J. The dust tail of asteroid (3200) Phaethon. *Astrophys. J.* **771,** L36 (2013).
17. Brown, P., Weryk, R. J., Wong, D. K. & Jones, J. A meteoroid stream survey using the Canadian Meteor Orbit Radar. I. Methodology and radiant catalogue. *Icarus* **195,** 317–339 (2008).

18. Brown, P., Wong, D. K., Weryk, R. J. & Wiegert, P. A meteoroid stream survey using the Canadian Meteor Orbit Radar. II: identification of minor showers using a 3D wavelet transform. *Icarus* **207,** 66–81 (2010).
19. Rivkin, A. S., Howell, E. S., Vilas, F. & Lebofsky, L. A. Hydrated minerals on asteroids: the astronomical record. *Asteroids* **III,** 235–253 (2002).
20. Hsieh, H. H. & Jewitt, D. A population of comets in the main asteroid belt. *Science* **312,** 561–563 (2006).
21. Küppers, M. *et al.* Localized sources of water vapour on the dwarf planet (1) Ceres. *Nature* **505,** 525–527 (2014).
22. Mainzer, A. *et al.* NEOWISE observations of near-Earth objects: preliminary results. *Astrophys. J.* **743,** 156 (2011).

Supplementary Information is available in the online version of the paper.

Author Contributions M.G. conceived the disruption model. M.G., A.M. and W.F.B. carried out orbital integrations using code modified by D.V. and A.M. R.J., B.B., M.G. and E.B. estimated observational biases for CSS. M.G. developed the code for fitting model parameters and carried out the fits. M.D. provided expertise on the WISE albedo analysis. M.G. wrote the paper with input from all authors.

Author Information The code for orbital integrations, SWIFT, is available at https://www.boulder.swri.edu/~hal/downloads. Reprints and permissions information is available at www.nature.com/reprints. The authors declare no competing financial interests. Readers are welcome to comment on the online version of the paper. Correspondence and requests for materials should be addressed to M.G. (mgranvik@iki.fi).